

Electronic properties of oligoacenes from first principles

Kerstin Hummer and Claudia Ambrosch-Draxl*

Institut für Physik, Universität Graz, Universitätsplatz 5, 8010 Graz, Austria

(Received 17 May 2005; revised manuscript received 19 August 2005; published 14 November 2005)

We present the electronic band structures and dielectric tensors for a series of crystalline linear oligoacenes—i.e., naphthalene, anthracene, tetracene, and pentacene—calculated within the density functional framework. The band dispersions, the effective charge carrier masses, and the optical response are discussed as a function of the oligomer length compared to previously reported calculations. The total band dispersions of the two topmost valence and lowest conduction bands are between 0.14 and 0.52 eV, which, however, are strongly anisotropic. Regarding the charge transport properties, the band dispersions are large enough for bandlike transport only along crystalline directions within the herringbone plane. Except for naphthalene, the conduction bands are more dispersive than the valence bands. This indicates that the electron transport is favored compared to hole migration. The revised stable pentacene single-crystal structure exhibits the largest conduction-band dispersions among the series. Consequently the effective electron masses in pentacene are only $0.8m_0$, whereas the hole masses are in the order of $1.3m_0$. The electronic and optical gaps and thus the onset of the optical response decrease almost linearly, when going from naphthalene to pentacene.

DOI: [10.1103/PhysRevB.72.205205](https://doi.org/10.1103/PhysRevB.72.205205)

PACS number(s): 71.20.Rv, 78.40.Me, 72.20.Jv, 71.15.Mb

I. INTRODUCTION

In recent plastic electronic research, not only have conducting polymers been the focus of interest, but also organic materials consisting of small π -conjugated molecules have experienced thorough investigations. Their applicability in innovative optoelectronic devices such as organic thin-film transistors^{1,2} is due to their ability to form well-defined molecular crystals. Thus these compounds allow for the preparation of crystalline thin films, which exhibit high-field-effect mobilities at room temperature. Particularly in pentacene thin-film transistors, high carrier mobilities for hole transport between 0.3 and 1.5 $\text{cm}^2/(\text{V s})$ have been observed.³ In view of their potential in such organic optoelectronic applications, a variety of measurements have been performed on the linear oligoacenes to determine their electronic and optical properties—e.g., charge carrier mobilities^{4,5} and photoconductivity.⁶ Concerning the former, recent theoretical investigations^{7–9} report different results for the pentacene band dispersion—i.e., the quantity that allows one to estimate the charge carrier mobilities.

Regarding the optical properties, the nature of the lowest optical transitions in such organic semiconductors has been of great interest and comprehensively studied in the past. *Ab initio* calculations successfully contributed to this puzzle, revealing the importance of the interchain interaction for the excitonic effects in polymers.^{10–12} In contrast to polymers, organic molecular crystals are built of finite molecules. Therefore, the electronic and optical properties are expected to differ from those of organic polymers. This added another motivation to investigate the dependence of the electronic properties and optical response on the oligomer length. The considered materials are the first four members in the group of linear oligoacenes—i.e., naphthalene (2A), anthracene (3A), tetracene (4A), and pentacene (5A). 5A is polymorph and crystallizes in different phases depending on the growth conditions and film thickness. Since higher charge carrier

mobilities are expected for the single-crystalline phase, this aspect is particularly important for the preparation of thin-film transistor devices. Therefore, we have extended our study by the recently revised pentacene single-crystal structure¹³ for comparison. Thereby, also the sensibility of the electronic properties on the minor structural changes becomes clear.

The thorough investigation of the oligoacenes' optical properties taking into account excitonic effects, which is published in Ref. 14, gives a clear picture of the nature of the lowest optical transitions and their dependence on the molecular size. In the present work we focus on the electronic properties of the oligoacenes. In particular their band structures are discussed with respect to the molecular size. In view of the transport properties the band dispersions are carefully analyzed and the effective charge carrier masses are evaluated. Their densities of states (DOS) as well as dielectric tensors are also presented.

II. COMPUTATIONAL DETAILS

A. Crystalline structure information

Each single oligoacene molecule consist of sp^2 -hybridized carbon atoms (C) and hydrogen atoms (H). In particular, each C forms three covalent σ bonds, the fourth valence electron resides in a $2p$ orbital perpendicular to the molecular plane generating the aromatic π -electron cloud. The oligoacene molecules are rather rigid and planar due to this aromatic type of bonding. This planarity is preserved in the crystalline environment. As example for the oligoacenes (nA), the anthracene molecule is depicted in Fig. 1. n in nA indicates the number of repeating phenyl rings and equals 2, 3, 4, and 5, for naphthalene, anthracene, tetracene, and pentacene, respectively. The black (gray) lines represent C—C (C—H) σ bonds, whereas the ellipses visualize the π -electron cloud.

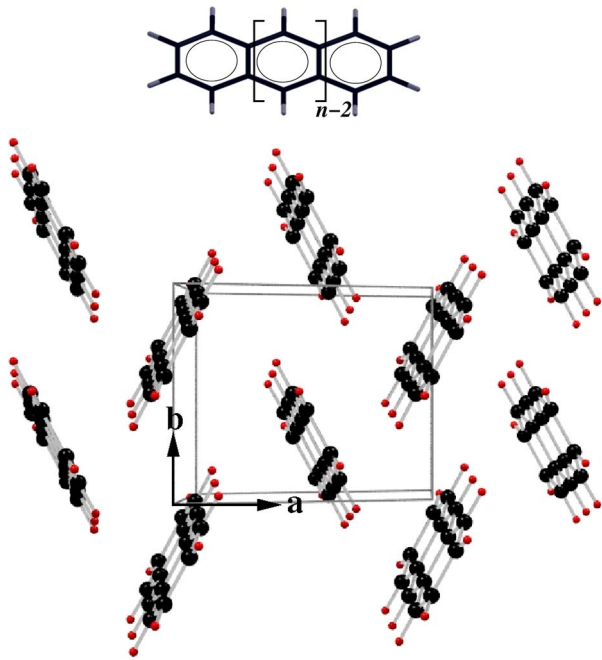


FIG. 1. (Color online) The anthracene (3A) molecule as well as the herringbone arrangement of two inequivalent molecules in the **ab** plane of crystalline 3A. The number of repeating phenyl rings is indicated by n in nA and equals 2, 3, 4, and 5, for naphthalene, anthracene, tetracene, and pentacene, respectively.

The lattice parameters of all the studied materials and their chemical formulas are given in Table I. At ambient conditions, 2A and 3A crystallize in the monoclinic structure $P2_1/a$, whereas 4A and 5A are characterized by the triclinic space group $P\bar{1}$. The main structural features of these materials are the herringbone arrangement of two inequivalent molecules in the **ab** plane (see Fig. 1) and a layered structure of molecules along the **c** axis, which is common for rigid rod-like molecules. According to the thorough structure investigations of 5A by Mattheus *et al.*,^{13,19} four different polymorphs have been recently characterized. In order to distinguish these structures the d spacing of the (001) reflection has been evaluated. Already in the 1960s, a single-crystal phase with a d spacing of 14.5 Å had been identified by Campbell *et al.*^{18,20} However, the more recent experiments of Holmes *et al.*²¹ and Mattheus *et al.*^{13,19} reveal that the stable

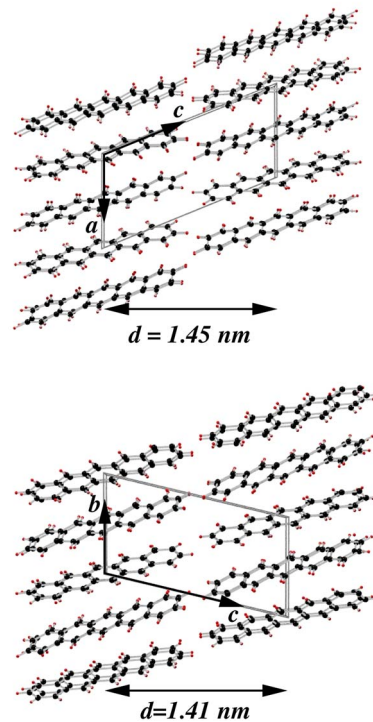


FIG. 2. (Color online) The **ac** plane of the pentacene crystal reported by Campbell *et al.* (Refs. 18 and 20) (top) and the revised structure by Mattheus *et al.* (Refs. 13 and 19) (bottom).

single-crystal pentacene phase has interchanged **a** and **b** axes and a much smaller d spacing of 14.1 Å. The lattice constants of the latter structure can be transformed into those reported by Campbell *et al.*, but the angles α and β differ, resulting in a deviation of the d spacing. For our calculations, we have used both these structures, which are in the following referred to as 5A-C and 5A-M, respectively. In Fig. 2 the **ac** plane of 5A-C (top) as well as the **bc** plane of the 5A-M structure (bottom) are shown to visualize the small structural differences. In addition to the change in the d spacing, the molecules corresponding to one layer are shifted with respect to the molecules of the neighboring layer. Moreover, the herringbone angle θ , which is defined as the angle between the normal vectors to the molecular planes of the two inequivalent molecules, is roughly 20° larger in 5A-M—i.e., 162.26° and 140.14° in 5A-M and 5A-C, respec-

TABLE I. Lattice parameters of the oligoacenes (Refs. 15–17) including two data sets for the pentacene single crystal structure, which are 5A-C (Ref. 18) and 5A-M, (Ref. 13) respectively.

Chemical formula	2A	3A	4A	5A-C	5A-M
	C ₁₀ H ₈	C ₁₄ H ₁₀	C ₁₈ H ₁₂	C ₂₂ H ₁₄	
a [Å]	8.24	8.56	7.98	7.93	6.266
b [Å]	6.00	6.04	6.14	6.14	7.775
c [Å]	8.66	11.18	13.57	16.03	14.53
α [deg]	90.0	90.0	101.3	101.9	76.475
β [deg]	122.9	124.7	113.2	112.6	87.682
γ [deg]	90.0	90.0	87.5	85.8	84.684

tively. At this point, we also want to comment on the pentacene thin-film structures in order to avoid confusion when comparing our pentacene results to literature data.^{8,9} Siegrist *et al.*²² determined a 5A phase, which is very similar to the $d=14.1$ Å structure previously reported by Holmes *et al.*²¹ Since their phase preferably appeared in vapor-phase deposited films under special growth conditions, it has been called a “V phase” in contrast to the “S phase” denoting the structure by Campbell *et al.* However, the so-called 5A “V phase” turned out to be the stable single-crystal structure, whereas the thin-film phases adopt d spacings of 14.4, 15.0, and 15.4 Å.^{13,19}

Concerning the analysis of the band structures below, we want to emphasize an important aspect resulting from the materials’ crystal symmetry. Due to the herringbone arrangement of the molecules, each band in the band structures appears doubled, forming a band pair. Besides some high-symmetry points in the irreducible wedge of the Brillouin zone (IBZ) (see Fig. 3), the bands of these pairs are nondegenerate, leading to band splitting.

B. Method of calculation

We apply the full-potential (FP) augmented plane-wave plus local orbitals (APW+lo) formalism²³ as implemented in the WIEN2k code²⁴ to perform the ground-state calculations. Exchange and correlation effects have been treated by the generalized gradient approximation (GGA).²⁵ The \mathbf{k} -space integrations have been carried out by an improved tetrahedron method²⁶ on a grid of six (five) \mathbf{k} points in the IBZ for 2A, 3A, 5A-C, and 5A-M (4A). Starting from the lattice parameters of nA given in Table I the internal geometry has been optimized; i.e., the atomic positions have been relaxed by minimizing the forces acting on the atoms to be less than 2 mRy/a.u. (0.05 eV/Å) in magnitude. In each self-consistent cycle, the atomic forces were converged better than 1 mRy/a.u., resulting in a total energy convergence of 0.1 mRy.

The oligoacene band structures have been computed on a discrete \mathbf{k} mesh along high-symmetry directions. Although the IBZ’s of the different structures are not identical, the chosen \mathbf{k} paths represent high-symmetry lines for all lattice types and thus allow for comparison of the band structures. The reciprocal coordinates of the high-symmetric points Γ , Y, Z, A, B, and D in units of $(2\pi/a, 2\pi/b, 2\pi/c)$ are (0,0,0), (0.5,0,0), (0,0,0.5), (0.5,0.5,0), (0,0.5,0), and (0.5,0.5,-0.5), respectively. Note that $\overline{\Gamma Y}$ ($\overline{\Gamma B}$) is parallel to the reciprocal crystalline \mathbf{a}^* (\mathbf{b}^*) axis, whereas $\overline{\Gamma Z}$ corresponds to the \mathbf{c}^* direction. The path along $\overline{\Gamma A}$ describes the \mathbf{k} -point sampling in the herringbone plane—i.e., the \mathbf{ab} plane (see last panel in Fig. 3).

The imaginary part of the dielectric tensor $\epsilon_2^{ij}(\omega)$ has been calculated within the random phase approximation²⁷ (RPA):

$$\epsilon_2^{ij}(\omega) = \frac{8\pi^2}{V(\omega - \Delta_c)^2} \sum_{v\mathbf{c}\mathbf{k}} \langle v\mathbf{k}|p_i|\mathbf{c}\mathbf{k} \rangle \langle \mathbf{c}\mathbf{k}|p_j|v\mathbf{k} \rangle \times \delta(\epsilon_{\mathbf{c}\mathbf{k}} - \epsilon_{v\mathbf{k}} + \Delta_c - \omega). \quad (1)$$

The indices v (c) and \mathbf{k} represent the valence (conduction)

band and a vector \mathbf{k} in the IBZ. V and ω stand for the unit-cell volume and the frequency of the incoming light, respectively, whereas i and j indicate the polarization direction of the optical response. $\langle v\mathbf{k}|p_i|\mathbf{c}\mathbf{k} \rangle$ are the optical dipole matrix elements, where p_i denotes the i th Cartesian component of the momentum operator. These matrix elements that provide the selection rules for $\epsilon_2^{ij}(\omega)$ have been computed on a dense grid of a $(13 \times 14 \times 9)$ \mathbf{k} points in an energy window from plus to minus 1.5 Ry with respect to the Fermi level.

The valence- and conduction-state energies $\epsilon_{v\mathbf{k}}$ and $\epsilon_{c\mathbf{k}}$ have been approximated by the Kohn-Sham eigenvalues corrected by a \mathbf{k} -independent self-energy (scissors operator Δ_c) (Ref. 28), such that the optical gap calculated by taking into account the electron-hole Coulomb interaction matches the experimentally observed one.¹⁴ The same Δ_c has also been applied to 5A-M. Further details on the APW+lo specific parameters, like muffin-tin radii, plane-wave cutoff, and $R_{\text{MT}}K_{\text{max}}$ as well as \mathbf{k} -point convergence tests for the optical dipole matrix elements, are summarized elsewhere.²⁹ The RPA does not account for the electron-hole interaction and thus is not able to describe excitonic effects, which can be achieved by solving the Bethe-Salpeter equation. Since the n dependence of the optical response is more strongly pronounced than the excitonic effects that are only important close to the optical gap, we have used the RPA for the aim of our study.

According to the monoclinic and triclinic symmetry of nA , the imaginary part of the frequency-dependent dielectric tensor consists of the Cartesian diagonal elements $\epsilon_2^{zz}(\omega)$, $\epsilon_2^{yy}(\omega)$, and $\epsilon_2^{xx}(\omega)$ and the additional off-diagonal components $\epsilon_2^{xy}(\omega)$, $\epsilon_2^{xz}(\omega)$, and $\epsilon_2^{yz}(\omega)$, respectively. In the monoclinic unit cells, the Cartesian axis \mathbf{y} (\mathbf{z}) is equivalent to the crystalline \mathbf{b} (\mathbf{c}) axis, while the \mathbf{a} axis deviates from \mathbf{x} by the monoclinic angle β . Therefore, $\epsilon_2^{yy}(\omega)$ and $\epsilon_2^{zz}(\omega)$ describe the \mathbf{b} - and \mathbf{c} -axis-polarized transitions, respectively. Due to the loss of the screw axis symmetry in triclinic 4A and 5A, only the \mathbf{c} axis remains parallel to the Cartesian \mathbf{z} axis. In order to allow for a comparison with experiments performed on crystalline samples, the Cartesian components of the dielectric tensors have been transformed into those corresponding to the crystalline axes.

III. RESULTS AND DISCUSSION

In the following sections the band structures and DOS of the investigated oligoacenes as well as the calculated electronic band gaps, band splittings, band dispersions, and effective charge carrier masses are presented. Our theoretical findings are compared to the results obtained within the tight-binding approximation by Cheng *et al.*⁷ and the recent first-principles results of Endres *et al.*⁸ and Tiago *et al.*⁹ The last section is devoted to the discussion of the dielectric tensors as a function of the molecular size.

A. Band structures and DOS

In Figs. 3 and 4 the band structures $E(\mathbf{k})$ and DOS of 2A, 3A, 4A, 5A-C, and 5A-M are depicted. The directions of high symmetry chosen for the \mathbf{k} -point sampling are illustrated in

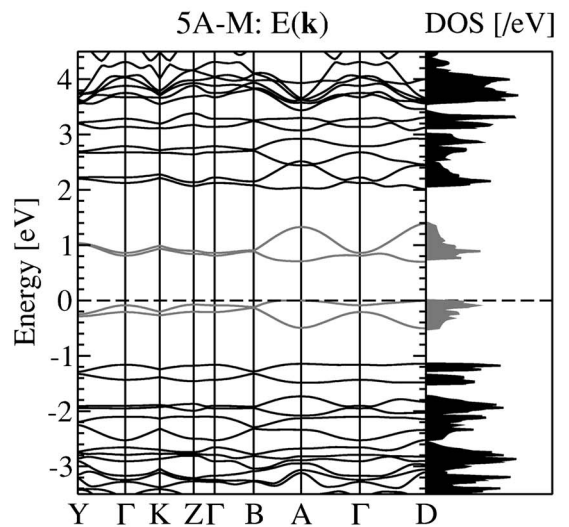
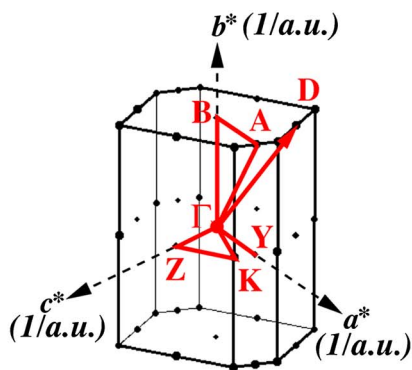
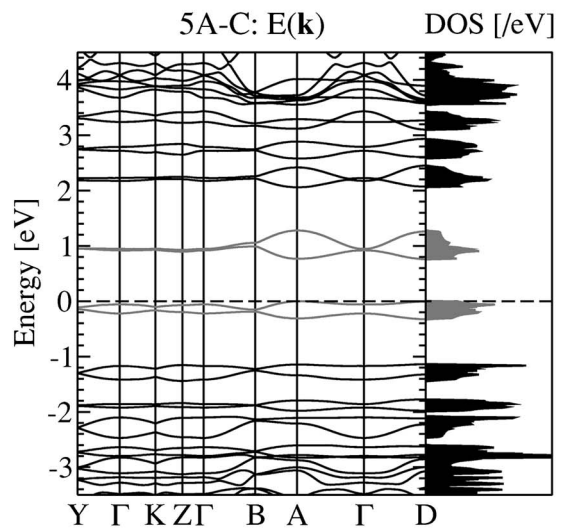
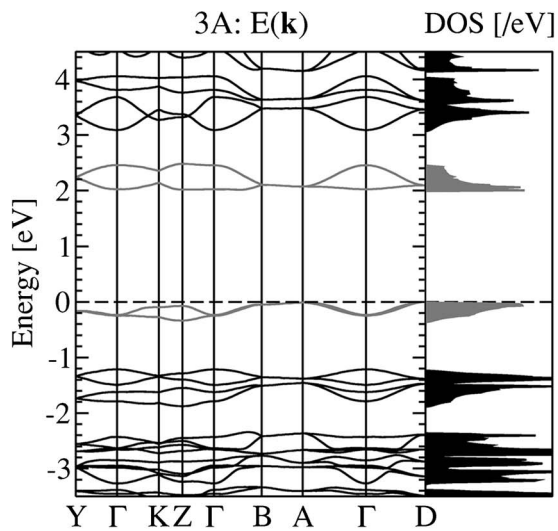
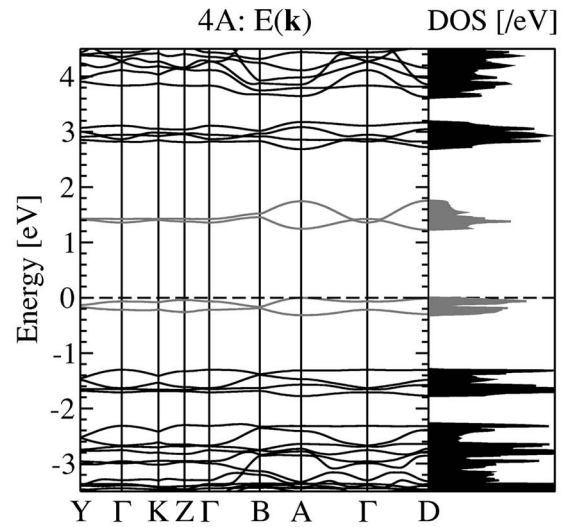
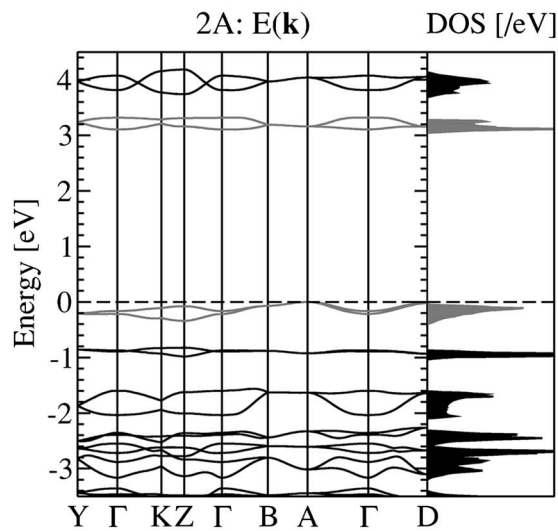


FIG. 3. (Color online) The band structures $E(\mathbf{k})$ and DOS of monoclinic 2A (top) and 3A (middle), as well as the IBZ of 3A (bottom) illustrating the \mathbf{k} path along which the energies have been calculated for the oligoacenes. The high-symmetry points in units of $(2\pi/a, 2\pi/b, 2\pi/c)$ are $\Gamma=(0,0,0)$, $Y=(0.5,0,0)$, $Z=(0,0,0.5)$, $A=(0.5,0.5,0)$, $B=(0,0.5,0)$, and $D=(0.5,0.5,-0.5)$. The Fermi level is indicated by the dashed line. The subbands of the VB and CB as well as their DOS are given in gray.

FIG. 4. Analogous to Fig. 3 from top to bottom: the band structures $E(\mathbf{k})$ and DOS of the triclinic systems 4A, 5A-C, and 5A-M.

TABLE II. The Kohn-Sham band gaps E_g^{GGA} of 2A, 3A, 4A, 5A-C, and 5A-M compared to experimentally observed values. (Refs. 30–40).

	2A	3A	4A	5A-C	5A-M
E_g^{GGA} [eV]	3.10	2.01	1.23	0.77	0.76
E_g^{expt}	5.0–5.4	3.9–4.2	2.9–3.4	2.2–2.4	

the bottom viewgraph of Fig. 3. The subbands corresponding to the uppermost valence-band (VB) pair and lowest conduction-band (CB) pair as well as their corresponding DOS are highlighted in gray in these figures. The high anisotropy of the band dispersions is a common feature within the series. Taking a closer look it is noticeable that the band structures of the monoclinic 2A and 3A are similar, but are clearly distinct from those of the triclinic compounds. This becomes particularly evident when analyzing the band splitting and band dispersions. Further, the band structure of 4A is alike that of 5A-C. However, the structural differences between 5A-C and 5A-M are apparent in their electron bands. When going from the monoclinic structures to the triclinic phases, the changes of the electron bands are significant. In the region between points B and D, (i) the subbands of the VB increase their splitting and change the sign of the curvature but become much flatter along the other directions, (ii) the degeneracy between B and A is lost, and (iii) the conduction bands increase their parabolicity and dispersion. According to (iii), the CB bandwidths W_{CB} increase within the series. At this point we want to emphasize that we define the bandwidth of a band pair as the energy range covered by the continuous region in the DOS, whereas the band dispersion is determined by the single subband. Thereby we clearly distinguish between these two quantities. Consequently, the bandwidth includes the band dispersion and/or band splitting, whichever is the determining one. In 5A-M, the sequence of a rather dispersed and a flat subband in the VB and vice versa in the CB is distinctive. The parabolic band features are also evident in the DOS corresponding to these bands.

Going from 2A to 5A-C (5A-M) we find 340, 337, 315, 324 (514) meV and 215, 467, 528, 518 (666) meV for W_{VB} and W_{CB} , respectively. While W_{VB} is roughly constant within the series, W_{CB} increases. In 5A-M both, W_{VB} and W_{CB} are significantly larger and solely determined by the band splitting at point D. In contrast, in 2A and 3A, W_{VB} is equal to the band dispersion of VB_2 . In the remaining cases the bandwidths are determined by the combination of band splitting and band dispersion. Recent GW calculations of the 5A-C and 5A-M structure presented by Tiago *et al.*⁹ yielded very similar values for W_{VB} as well as W_{CB} , which makes us confident that GW calculations for the remaining members of the series would probably give similar results to those obtained with density functional theory (DFT) within the APW+lo formalism. In comparison to the bandwidths reported by Cheng *et al.*⁷ our values are smaller. Since the band dispersion of each subband and their splitting contribute to the bandwidths, the proper description of the band anisotropy is important. We further refer to these differences in the section below, when we discuss the band dispersions and splitting in detail.

1. Band gaps

The Kohn-Sham band gaps of all oligoacenes deduced from the band structures are listed in Table II. Compared to experiment^{30–40} these values are underestimated as expected from DFT calculations. However, our results perfectly reproduce the experimentally observed decrease of the band gap with increasing oligomer length n , which is also illustrated in the left panel of Fig. 5. By plotting the band gap versus the inverse oligomer length a nearly linear relation is obtained for the oligoacenes similarly to the oligophenylenes.^{41,42} As can be seen from the right panel in Fig. 5, this linearity is broken by a kink that marks the transition from monoclinic unit cells to triclinic space groups. While in the monoclinic structures, the fundamental band gaps are indirect gaps, in triclinic 4A, 5A-C, and 5A-M the lowest direct gaps occur at point D. The lowest direct energy gaps in 2A and 3A are approximately 0.06 eV larger than the fundamental ones. Since the direct gaps evaluated at these points differ only by less than 1 meV, the calculation hardly allows one to resolve between A and D. Tiago *et al.*⁹ reported a Kohn-Sham gap of 0.8 eV and 0.7 eV for 5A-C and 5A-M, respectively, which is also reproduced by our calculations. The band gap of the 5A-C structure at the Γ point is 0.98 eV, which is in excellent agreement with the 0.95 eV reported by Endres *et al.*⁸ The corresponding value for 5A-M is 0.97 eV.

2. Band splittings

Let us now focus on the band splitting, which has also been evaluated from the band structures. Figure 6 shows the band splitting of the VB and CB at high-symmetry points in the IBZ as a function of the oligomer length n . While in 2A, the VB and CB exhibit the largest splitting at points Z and Γ , respectively, in 3A, the maximum splitting of both bands is

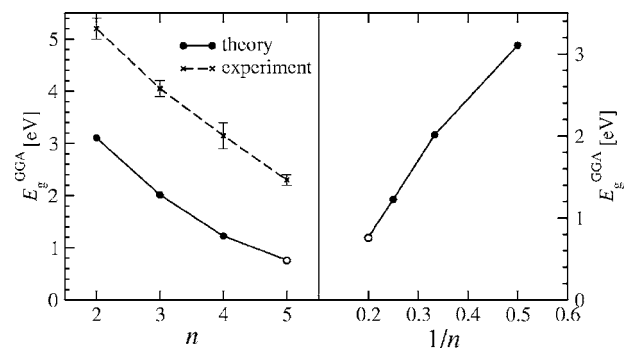


FIG. 5. The GGA energy gap E_g^{GGA} compared to data available in literature (Refs. 30 and 40) as a function of the oligomer length n (left) as well as a function of the inverse oligomer length $1/n$ (right). The open symbols correspond to the 5A-M structure.

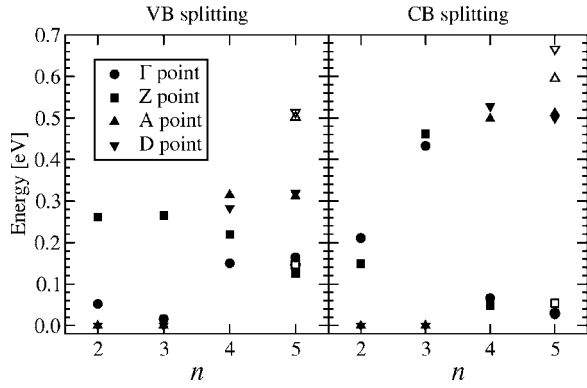


FIG. 6. The band splitting of the highest occupied VB (left) and the lowest unoccupied CB (right) at high-symmetry points in the IBZ as a function of the oligomer length n . The open symbols correspond to the $5A-M$ structure.

obtained at point Z. In contrast, the VB in 4A and the CB in 5A-C exhibit the largest splitting at point A, whereas the CB in 4A and the VB in 5A-C reach the maximum splitting at point D. In 5A-M the splitting of all subbands (open symbols in Fig. 6) is largest at the D point. Note that the VB and CB of 2A and 3A are degenerate at A and D. In 5A-C the band splitting of the VB (CB) at the points Γ , Z, and A (i.e., K in Ref. 8) is 164 (27) meV, 135 (31) meV, and 311 (512) meV, respectively. These values agree within 3% with the values extracted from the DFT calculations of Endres *et al.*,⁸ except that the splitting of the CB at A is roughly 20% larger. The analogous values of splitting at Γ and Z (A) reported by Cheng *et al.*,⁷ which have been obtained by a tight-binding approximation to the band structure, are much higher (smaller) compared to both DFT results. This difference is attributed to the inherent difference between the theoretical approaches. While the latter takes into account the full three-dimensional (3D) crystalline environment, it is not fully considered in case of the semiempirical tight-binding calculations.

3. Band dispersions

In the following we discuss the band dispersions of the oligoacenes. These quantities can be related to the effective carrier masses and further to the charge carrier mobilities. In Table III, we summarize the band dispersions for the single bands close to the Fermi level, which are relevant for the charge transport in the directions corresponding to the reciprocal crystalline axes \mathbf{a}^* , \mathbf{b}^* , and \mathbf{c}^* and in the herringbone packing direction ($\mathbf{a}^* + \mathbf{b}^*$). These directions are equivalent to $\bar{\Gamma Y}$, $\bar{\Gamma B}$, $\bar{\Gamma Z}$, and $\bar{\Gamma A}$, respectively. The values corresponding to the largest dispersions among these directions are highlighted with bold letters in Table III. Additionally, the dispersion is evaluated for the whole band as energy difference between each single-band minimum and maximum. In order to distinguish between the subbands of the VB and CB, we introduce a subscript, which denotes the sequence of the single bands downwards and upwards in energy from the Fermi level. From Table III it becomes clearer that the monoclinic and triclinic band structures are different, whereas

TABLE III. The band dispersion of 2A, 3A, 4A, 5A-C, and 5A-M calculated along $\bar{\Gamma Y}$, $\bar{\Gamma B}$, $\bar{\Gamma Z}$, and $\bar{\Gamma A}$ and for the whole band for VB₂, VB₁, CB₁, and CB₂.

Band dispersion [meV]		$\bar{\Gamma Y}$	$\bar{\Gamma B}$	$\bar{\Gamma Z}$	$\bar{\Gamma A}$	Whole band
2A	VB ₂	11	148	123	217	340
	VB ₁	44	96	87	165	208
	CB ₁	135	85	54	54	136
	CB ₂	77	131	9	158	165
3A	VB ₂	87	201	89	240	337
	VB ₁	72	188	163	224	234
	CB ₁	221	89	6	51	228
	CB ₂	212	351	27	382	410
4A	VB ₂	43	28	41	99	142
	VB ₁	65	97	28	68	165
	CB ₁	54	97	20	155	230
	CB ₂	6	95	2	330	341
5A-C	VB ₂	75	33	3	91	177
	VB ₁	53	94	15	57	151
	CB ₁	30	71	23	152	229
	CB ₂	9	110	19	334	352
5A-M	VB ₂	88	60	9	277	344
	VB ₁	142	22	10	82	225
	CB ₁	188	68	21	107	305
	CB ₂	185	54	46	458	522

those belonging to the same space group exhibit similarities. In both 2A and 3A, the band dispersions of VB₂, VB₁, and CB₂ are largest along $\bar{\Gamma A}$ ($\mathbf{a}^* + \mathbf{b}^*$), but CB₁ is highly dispersive along $\bar{\Gamma Y}$ (\mathbf{a}^*). When going from 2A to 3A the band dispersions increase in most of the directions considered. In contrast, for each direction the values for 4A and 5A-C are similar in magnitude. In particular, their valence bands are less dispersed than those of the monoclinic phases. Except along $\bar{\Gamma A}$ the lowest unoccupied conduction bands of the triclinic structures exhibit band dispersions comparable to 3A. In 4A and 5A-C, the band dispersion of VB₁ is largest along $\bar{\Gamma B}$, while CB₁, CB₂, and VB₂ reach their maximum between Γ and A. All these directions of largest dispersion are perpendicular to the long molecular axis, which is approximately the \mathbf{c}^* direction ($\bar{\Gamma Z}$).

When now focusing on the 5A-M values, the minor structural changes, in particular the increased herringbone angle, are significant for the band features. From a general point of view, the bands are clearly more dispersive in 5A-M, exhibiting the largest total subband dispersions within the series of oligoacenes (see last column of Table III). Note that in comparison to 5A-C, the \mathbf{a} and \mathbf{b} crystalline axes are interchanged in 5A-M. Therefore the band dispersion of VB₁ (0.14 eV) is largest along $\bar{\Gamma Y}$ in 5A-M, but along $\bar{\Gamma B}$ in 5A-C. The dispersion of CB₁ is also maximal in $\bar{\Gamma Y}$ and of similar magnitude—i.e., 0.19 eV. In turn, the VB₂ and CB₂ dispersions are still highest in the herringbone packing direc-

tion. Previous investigations of the structural and electronic properties of anthracene⁴³ and oligophenylenes⁴⁴ as well as fluorene⁴⁵ under pressure have revealed that the intermolecular interactions, which are mainly π - π interactions, are governed by the herringbone arrangement of the molecules. Furthermore, increasing the herringbone angle significantly enhances the intermolecular interaction and thus the band dispersion in the herringbone plane. Based on these findings, we conclude that the enhanced band dispersion along $\bar{\Gamma}Y$ and the herringbone plane can be related to the increase of the herringbone angle in 5A-M compared to 5A-C. Coherent bandlike transport is related to reasonably large band dispersion, which is highly sensitive to the molecular arrangement. For this reason, in particular the structural-induced increase in the 5A-M material shown here is an important issue for device applications. For example, the superior hole transport that has been observed in the pentacene thin-film transistors^{3,46,47} may be understood in terms of the band structure of the underlying pentacene thin-film phase.

When comparing our FP-APW band dispersions of 5A-C with the pseudopotential calculation of Endres *et al.*,⁸ we find an overall agreement for all considered directions listed in Table III. The significantly large values of the CB subband dispersions in the $(\mathbf{a}^* + \mathbf{b}^*)$ direction is also confirmed. Small deviations may be attributed to a denser \mathbf{k} -point sampling used for the structure relaxation in our FP-APW calculation.

In summary we can conclude from the band structure analysis that (i) the band structures of the monoclinic materials are different from those of the triclinic compounds, (ii) the intermolecular interaction is less pronounced in the \mathbf{c} direction, resulting in flatter bands along $\bar{\Gamma}Z$, and (iii) the largest band dispersions are exhibited in the herringbone plane. The latter two points apply to all investigated oligoacenes and, as a consequence of (iii), the highest charge carrier mobilities are expected along directions in the (\mathbf{ab}) plane. These conclusions have also been drawn from the semiempirical quantum-chemical method presented in Ref. 7. However, the details of their band structures do not sufficiently agree with our *ab initio* results. In particular, the latter show that strongly pronounced differences in the subband anisotropy are exhibited in these materials. Consequently, the tight-binding approximation to the band dispersions⁷ yields values generally larger than our *ab initio* findings, leading to an overestimation of the bandwidths. Moreover, in the former work a significant increase of both the VB and CB total bandwidths with the oligomer length is observed, which is not reproduced by the FP-APW method. We believe that the various differences in the two approaches are responsible for these discrepancies: Besides from using a semiempirical quantum-chemical method, Ref. 7 does not fully take into account the 3D periodicity, but only considers a molecular cluster. The full 3D environment is, however, crucial for a proper description of the electronic properties. This is also supported by the fact that the *ab initio* pentacene bandwidths reported by Endres *et al.*⁸ as well as Tiago *et al.*⁹ are in good agreement with our findings.

B. Effective charge carrier masses

The nature of charge carrier transport in organic crystals is still under vivid discussion.^{7,8,48-50} Cheng *et al.*⁷ concluded

TABLE IV. Effective electron (m_e^*) and hole (m_h^*) mass as a function of the oligomer length estimated at points A and D. The plus (minus) sign indicates the positive (negative) curvature of the regarding band. m_0 denotes the electron rest mass. The values in parentheses correspond to the left branch of the parabolic band.

	At point A		At point D	
	$m_h^*m_0$	$m_e^*m_0$	$m_h^*m_0$	$m_e^*m_0$
2A	-2.08	2.53	-2.40	1.68
3A	-2.32	1.22	2.02	-1.21
4A	5.61(2.65)	-1.37(-1.22)	6.22	-1.19
5A-C	4.79(2.28)	-1.56(-1.30)	4.46	-1.36
5A-M	1.37(0.88)	-0.93(-0.97)	1.44	-0.77

from their semiempirical calculations that the simple band model is applicable for temperatures only up to 100 K and that polaronic effects are important beyond. Nevertheless, the large dispersions along $\bar{\Gamma}A$ ($W \ll k_B T$) indicate that coherent, bandlike transport is possible. In 2A one can expect from the larger band dispersions of the VB₁ compared to CB₁ that the hole transport is favored, whereas in 3A the hole and electron mobilities should be similar. However, the band-to-band transition located at point A (D) is only slightly (0.06 eV) larger than the (indirect) band gap. Hence, VB₁ (CB₁) and VB₂ (CB₂) are degenerate at these points. Thus the VB₂ and CB₂ could possibly contribute to the charge carrier transport. The dispersion of CB₂ is large along $\bar{\Gamma}A$ ($\bar{\Gamma}D$) and in particular larger than that of VB₁ and VB₂.

When switching now to the triclinic systems, the important fact is that these structures exhibit large splittings between VB₁ (CB₁) and VB₂ (CB₂) at point D, where also the lowest band-to-band transition occurs. However, VB₁ and CB₁ are rather flat, yielding large carrier masses. In contrast, the effective masses resulting from the VB₂ and CB₂ dispersions are much lower, which is in agreement with experimental findings. We assume that the small band gap in combination with the highly dispersed VB₂ and CB₂ controls the outstanding transport properties in pentacene.¹

According to the simple approach known for the parabolic bands in inorganic semiconductors the charge carrier mobility is inversely proportional to the effective mass m^* , which in turn depends on the inverse of the band dispersion:

$$\frac{1}{m^*} = \frac{1}{\hbar^2} \frac{d^2 E(\mathbf{k})}{d\mathbf{k}^2}. \quad (2)$$

In order to estimate the effective electron (hole) mass m_e^* (m_h^*) we have fitted the oligoacene bands, which are possibly involved in the charge carrier transport to Eq. (2). These are in particular VB₂ and CB₂ at the points A and D towards $\bar{\Gamma}$. The corresponding data are summarized in Table IV, where the values given in parenthesis correspond to the parabolic branch A towards B. As evident from the numbers given in Table IV, m_e^* is generally smaller than m_h^* . When going from 2A to 5A-M, m_e^* clearly decreases within the series,

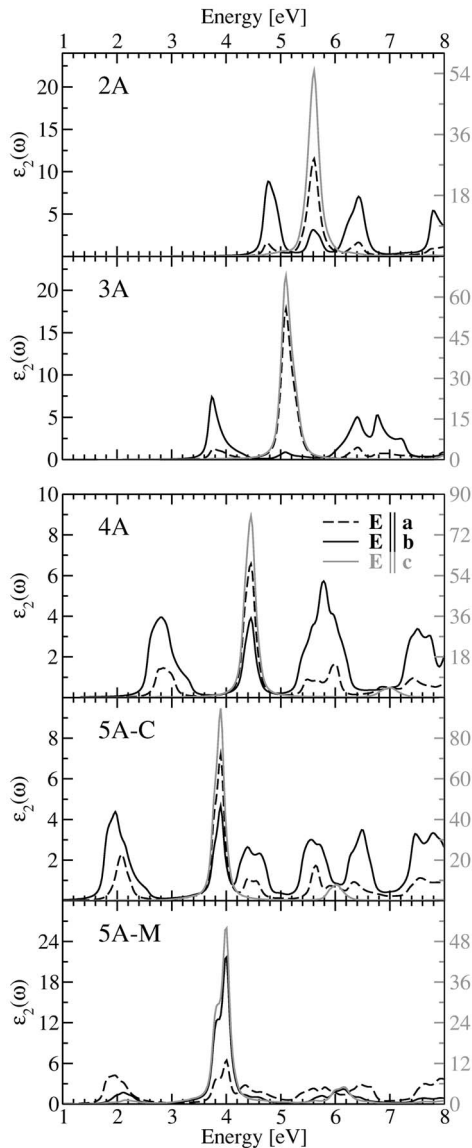


FIG. 7. Linear optical response $\epsilon_2(\omega)$ to incoming light with an electric field vector \mathbf{E} parallel to the crystal axes a , b , and c , respectively. A lifetime broadening of 0.05 eV has been included. The amplitude of the strong c -polarized absorption given in gray is plotted against the right y axis.

whereas m_h^* is significantly smaller in 2A and 3A compared to 4A and 5A-C/5A-M. When comparing 5A-C and 5A-M, both m_h^* and m_e^* are drastically reduced. Within the series, the smallest effective masses are estimated for 5A-M—i.e., $(0.8 \pm 0.1)m_0$ and $(1.3 \pm 0.4)m_0$ for m_e^* and m_h^* , respectively. These results are consistent with the calculations reported in Ref. 51.

C. Linear optical response

In the following we present the calculated dielectric tensors for the series of oligoacenes as a function of the molecular size and the polarization of the exciting radiation. In Fig. 7 the three components of $\epsilon_2(\omega)$ —i.e., the response to incoming light with an electric field vector \mathbf{E} parallel to the

crystal axes a , b , and c —are depicted. The optical transition with the strongest oscillator strength—i.e., the response to c -polarized light—is plotted in gray and related to the right y axis. For clarity, the two y axes have been differently scaled for each material. Take this into account when comparing the peak heights (oscillator strengths). As has been shown for anthracene⁵² the lowest optical response in all linear oligoacenes is generated by b -axis-polarized light and has rather weak oscillator strength. The dominant c -axis-polarized transition appears at higher energies. This behavior of the oligoacenes is clearly different from the oligophenylenes⁴⁴ and fluorene,⁴⁵ which have been previously studied. The a component of $\epsilon_2(\omega)$ plays a minor role and bears a contribution of the c component. The latter is also the case for the b component of the triclinic structures. In all oligoacenes the RPA onset matches the smallest direct band gap, reflecting that this optical absorption process is an allowed interband transition. When going from 2A to 5A-C (5A-M) the absorption onset is shifted to lower energies (redshift), which is in accordance with the reduction of the band gap. This redshift, however, is less pronounced for the c -axis-polarized transition. When comparing 5A-C and 5A-M we point out that due to the different axis assignment (see Table I), the a and b components of $\epsilon_2(\omega)$ are interchanged. A main difference is found in the position and shape of the c -axis-polarized peak. In 5A-M it is slightly shifted to higher energies, whereas a distinct shoulder is found at the position of the 5A-C peak.

IV. CONCLUSIONS

In our comprehensive *ab initio* investigation of the electronic properties of linear oligoacenes, we have addressed the question as to how these properties depend on the molecular size. From a detailed analysis of the band structures we are able to conclude that the conduction bands exhibit dispersions between 0.14 and 0.52 eV, whereas those of the valence bands are in the range of 0.14–0.34 eV. The largest band dispersions are found in directions within the herringbone plane. In contrast, the bands are rather flat along the crystalline c axis, which is the direction of the layer formation in these crystals with their molecules aligning to their long axis. The increase of the herringbone angle in 5A-M compared to 5A-C significantly alters the band structure; in particular, the band dispersions are enhanced in the herringbone plane in 5A-M. The fact that the electronic band gap is much smaller in 5A-M compared to 3A in combination with the rather wide valence and conduction bands in the herringbone plane can explain the superior transport properties (charge carrier generation and carrier mobilities) found for pentacene. The effective electron masses estimated from the band dispersions are drastically reduced within the series. The effective hole masses obtained for the monoclinic structures are smaller than those found in 4A and 5A-C. From a comparison to other theoretical approaches we conclude that the consideration of the full periodicity is very important for a proper description of the electronic properties of organic

molecular crystals. Regarding the application in thin-film transistors, detailed knowledge of the underlying crystal structure is crucial for the understanding of the electronic and optical properties. For this reason a theoretical investigation of the tetracene and pentacene thin-film polymorphs is the subject of future work.

ACKNOWLEDGMENTS

The authors would like to acknowledge the support of the Austrian Science Fund (Project No. 16227-PHY) and funding from the EU RT network "EXCITING", Contract No. HPRN-CT-2002-00317.

-
- *Electronic address: claudia.ambrosch@uni-graz.at; URL: <http://physik.uni-graz.at/~cad/>
- ¹C. D. Dimitrakopoulos and D. J. Mascaró, IBM J. Res. Dev. **45**, 11 (2001).
 - ²L. Torsi, N. Cioffi, C. D. Franco, L. Sabatini, P. G. Zamboni, and T. Bleve-Zacheo, Solid-State Electron. **45**, 1479 (2001).
 - ³S. Nelson, Y.-Y. Lin, D. J. Gundlach, and T. N. Jackson, Appl. Phys. Lett. **72**, 1854 (1998).
 - ⁴N. Karl, Synth. Met. **133–134**, 649 (2003).
 - ⁵N. Karl and J. Marktanner, Mol. Cryst. Liq. Cryst. Sci. Technol., Sect. A **355**, 149 (2001).
 - ⁶Z. Rang, A. Haraldsson, D. M. Kim, P. P. Ruden, M. I. Nathan, R. J. Chesterfield, and C. D. Frisbie, Appl. Phys. Lett. **79**, 2731 (2001).
 - ⁷Y. C. Cheng, R. J. Silbey, D. A. da Silva Filho, J. P. Calbert, J. Cornil, and J. L. Brédas, J. Chem. Phys. **118**, 3764 (2003).
 - ⁸R. G. Endres, C. Y. Fong, L. H. Yang, G. Witte, and C. Wöll, Comput. Mater. Sci. **29**, 362 (2004).
 - ⁹M. L. Tiago, J. E. Northrup, and S. G. Louie, Phys. Rev. B **67**, 115212 (2003).
 - ¹⁰J.-W. van der Horst, P. A. Bobbert, M. A. J. Michels, G. Brocks, and P. J. Kelly, Phys. Rev. Lett. **83**, 4413 (1999).
 - ¹¹A. Ruini, M. J. Caldas, G. Bussi, and E. Molinari, Phys. Rev. Lett. **88**, 206403 (2002).
 - ¹²P. Puschnig and C. Ambrosch-Draxl, Phys. Rev. Lett. **89**, 056405 (2002).
 - ¹³C. C. Mattheus, A. B. Dros, J. Baas, A. Meetsma, J. L. de Boer, and T. T. M. Palstra, Acta Crystallogr., Sect. C: Cryst. Struct. Commun. **C57**, 939 (2001).
 - ¹⁴K. Hummer and C. Ambrosch-Draxl, Phys. Rev. B **71**, 081202(R) (2005).
 - ¹⁵D. W. J. Cruickshank, Acta Crystallogr. **10**, 504 (1957).
 - ¹⁶R. Mason, Acta Crystallogr. **17**, 547 (1964).
 - ¹⁷J. M. Robertson, V. C. Sinclair, and J. Trotter, Acta Crystallogr. **14**, 697 (1961).
 - ¹⁸R. B. Campbell, J. M. Robertson, and J. Trotter, Acta Crystallogr. **14**, 705 (1961).
 - ¹⁹C. C. Mattheus, A. B. Dros, J. Baas, G. T. Oostergetel, A. Meetsma, J. L. de Boer, and T. T. M. Palstra, Synth. Met. **138**, 475 (2003).
 - ²⁰R. B. Campbell, J. M. Robertson, and J. Trotter, Acta Crystallogr. **15**, 289 (1962).
 - ²¹D. Holmes, S. Kumaraswamy, A. Matzger, and K. P. C. Vollhardt, Chem.-Eur. J. **5**, 3399 (1999).
 - ²²T. Siegrist, C. Kloc, J. H. Schön, B. Batlogg, R. C. Haddon, S. Berg, and G. A. Thomas, Angew. Chem., Int. Ed. **40**, 1732 (2001).
 - ²³E. Sjöstedt, L. Nordström, and D. J. Singh, Solid State Commun. **114**, 15 (2000).
 - ²⁴P. Blaha, K. Schwarz, G. K. H. Madsen, D. Kvasnicka, and J. Luitz, computer code WIEN2k (Vienna University of Technology, Vienna, 2001).
 - ²⁵J. P. Perdew, K. Burke, and M. Ernzerhof, Phys. Rev. Lett. **77**, 3865 (1996).
 - ²⁶P. E. Blöchl, O. Jepsen, and O. K. Andersen, Phys. Rev. B **49**, 16223 (1994).
 - ²⁷H. Ehrenreich and M. H. Cohen, Phys. Rev. **115**, 786 (1959).
 - ²⁸R. W. Godby, M. Schlüter, and L. J. Sham, Phys. Rev. B **37**, 10159 (1988).
 - ²⁹K. Hummer, *On the Electro-optical Properties of Oligo-acenes* (Shaker-Verlag, Aachen, 2004).
 - ³⁰Y. Isono, E. Morikawa, and M. Kotani, Chem. Phys. Lett. **125**, 344 (1986).
 - ³¹C. L. Braun and G. M. Dobbs, J. Chem. Phys. **53**, 2718 (1970).
 - ³²R. Silbey, J. Jortner, M. T. Vala, Jr., and S. A. Rice, J. Chem. Phys. **42**, 2948 (1965).
 - ³³A. I. Belkind and V. V. Grechov, Phys. Status Solidi A **26**, 377 (1974).
 - ³⁴H. Bässler and H. Killesreiter, Phys. Status Solidi B **53**, 183 (1972).
 - ³⁵L. Sebastian, G. Weiser, G. Peter, and H. Bässler, Chem. Phys. **75**, 103 (1983).
 - ³⁶N. Geacintov and M. Pope, J. Chem. Phys. **50**, 814 (1969).
 - ³⁷H. Bässler and H. Killesreiter, Mol. Cryst. Liq. Cryst. **24**, 21 (1973).
 - ³⁸E. A. Silinsh, V. A. Kolesnikov, I. J. Muzikante, and D. R. Balode, Phys. Status Solidi B **113**, 379 (1982).
 - ³⁹L. Sebastian, G. Weiser, and H. Bässler, Chem. Phys. **61**, 125 (1981).
 - ⁴⁰E. A. Silinsh, *Organic Molecular Crystals* (Springer-Verlag, Berlin, 1980).
 - ⁴¹A. Niko, F. Meghdadi, C. Ambrosch-Draxl, P. Vogl, and G. Leising, Synth. Met. **76**, 177 (1996).
 - ⁴²P. Puschnig and C. Ambrosch-Draxl, Phys. Rev. B **60**, 7891 (1999).
 - ⁴³K. Hummer, P. Puschnig, and C. Ambrosch-Draxl, Phys. Rev. B **67**, 184105 (2003).
 - ⁴⁴P. Puschnig, K. Hummer, C. Ambrosch-Draxl, G. Heimel, M. Oehzelt, and R. Resel, Phys. Rev. B **67**, 235321 (2003).
 - ⁴⁵G. Heimel, K. Hummer, C. Ambrosch-Draxl, W. Chunwachirasiri, M. J. Winokur, M. Hanfland, M. Oehzelt, A. Aichholzer, and R. Resel (unpublished).
 - ⁴⁶C. D. Dimitrakopoulos, A. R. Brown, and A. Pomp, J. Appl. Phys. **80**, 2501 (1996).
 - ⁴⁷C. D. Dimitrakopoulos, S. Purushothaman, J. Kymissis, A. Callegari, and J. M. Shaw, Science **283**, 822 (1999).
 - ⁴⁸J. L. Brédas, J. P. Calbert, D. A. da Silva Filho, and J. Cornil, Proc. Natl. Acad. Sci. U.S.A. **99**, 5804 (2002).

- ⁴⁹K. Hannewald, V. M. Stojanović, J. M. T. Schellekens, P. A. Bobbert, G. Kresse, and J. Hafner, *Phys. Rev. B* **69**, 075211 (2004).
- ⁵⁰K. Hannewald and P. A. Bobbert, *Phys. Rev. B* **69**, 075212 (2004).

- ⁵¹G. A. de Wijs, C. C. Mattheus, R. A. de Groot, and T. T. M. Palstra, *Synth. Met.* **139**, 109 (2003).
- ⁵²K. Hummer, P. Puschnig, and C. Ambrosch-Draxl, *Phys. Rev. Lett.* **92**, 147402 (2004).